# PROCEEDINGS OF SPIE

# Optimal experimental design to position transducers in ultrasound breast imaging

Naiara Korta Martiartu, Christian Boehm, Nicolas Vinard, Ivana Jovanović Balic, Andreas Fichtner

SPIE.

# Optimal experimental design to position transducers in ultrasound breast imaging

Naiara Korta Martiartu[a], Christian Boehm[a], Nicolas Vinard[a], Ivana Jovanović Balic[b], and Andreas Fichtner[a]

[a]Department of Earth Sciences, ETH Zurich, CH-8092 Zurich, Switzerland
[b]SonoView Acoustic Sensing Technologies, CH-2560 Nidau, Switzerland

## ABSTRACT

We present methods to optimize the setup of a 3D ultrasound tomography scanner for breast cancer detection. This approach provides a systematic and quantitative tool to evaluate different designs and to optimize the configuration with respect to predefined design parameters. We consider both, time-of-flight inversion using straight rays and time-domain waveform inversion governed by the acoustic wave equation for imaging the sound speed. In order to compare different designs, we measure their quality by extracting properties from the Hessian operator of the time-of-flight or waveform differences defined in the inverse problem, i.e., the second derivatives with respect to the sound speed. Spatial uncertainties and resolution can be related to the eigenvalues of the Hessian, which provide a good indication of the information contained in the data that is acquired with a given design. However, the complete spectrum is often prohibitively expensive to compute, thus suitable approximations have to be developed and analyzed. We use the trace of the Hessian operator as design criterion, which is equivalent to the sum of all eigenvalues and requires less computational effort. In addition, we suggest to take advantage of the spatial symmetry to extrapolate the 3D experimental design from a set of 2D configurations. In order to maximize the quality criterion, we use a genetic algorithm to explore the space of possible design configurations. Numerical results show that the proposed strategies are capable of improving an initial configuration with uniformly distributed transducers, clustering them around regions with poor illumination and improving the ray coverage of the domain of interest.

**Keywords:** experimental design, ultrasound tomography, waveform inversion, straight-ray inversion, resolution analysis, eigenvalue spectrum

## 1. INTRODUCTION

Developing tomography-based ultrasound technologies for early breast cancer detection – particularly to improve cancer detection for patients with dense breast tissue – has been an active field of research within the last decade.[1–5] In contrast to conventional hand-held ultrasound systems, in which reflected and backscattered information is used to obtain B-mode images, Ultrasound Computed Tomography (USCT) uses both transmitted and reflected signals to create images of the tissue's acoustic properties, such as sound speed, attenuation, compressibility, or scatter density. These quantitative images are particularly useful for characterizing breast tissue and differentiating between benign and malignant lesions as demonstrated by Greenleaf et al.[6]

There are different approaches to model the propagation of ultrasonic waves for USCT, ranging from computing the times-of-flight to the numerical simulation of the wave equation. Ray-based time-of-flight approaches are widely used for sound speed and attenuation reconstructions.[7,8] This appears to be a promising approach for several proposed scanning devices which operate in frequency ranges of 1-3 MHz.[9–12] However, with the

---

need to improve the diagnostic accuracy of USCT and to incorporate also diffraction and multiple scattering effects, on the one hand, and the availability of high-performance computing architectures, on the other hand, waveform tomography has become a promising alternative.[13–15] Pratt et al.[13] introduced frequency domain waveform tomography for 2D layer-by-layer systems using *in vivo* datasets showing promising results. Such 2D systems reduce the computational and experimental cost considerably, and they have become available for clinical evaluation.[5,9,10] Furthermore, Goncharsky et al.[15] recently showed in numerical tests that fully 3D devices, which have the advantage to also include out-of-plane scattering and refraction, improve the accuracy of the reconstructions, particularly when applying waveform tomography. Moreover, the authors suggested that low-frequency transducers (0.3-0.5 MHz) could even reduce the computational and experimental cost inherent to the problem, because it involves the use of a relatively small number of ultrasound sources.

While these studies show the great potential of waveform tomography, developing a cost-effective and accurate 3D USCT system for real applications still remains a challenge. In particular, this leads to an open research question: how should we design the locations of the transducers in a 3D experimental setup to maximize the information contained in the measured ultrasound data? While one might intuitively choose a configuration in which transducers are uniformly distributed on the device, a study by Gemmeke et al.[16] has shown how non-uniform transducer locations could improve the resolution in sound speed reconstructions. The goal of this paper is to introduce a systematic and quantitative framework to evaluate different designs and to optimize the configuration with respect to predefined design parameters.

Methods for Optimal Experimental Design (OED) have been applied successfully in many different fields, e.g., in seismic exploration to optimize the survey design for tomography problems.[17] Similar to ultrasound tomography, the goal is to find a configuration of emitting and receiving transducers such that the collected data contains information that best resolve certain model parameters once the experiment is executed. Such methods typically depend on the model-data relationship[18,19] and they can be extremely computationally expensive for nonlinear problems.

In this work, we propose a computationally tractable method to optimize transducer locations for 3D ultrasound tomography scanning systems. Here, we consider a hemispherically shaped measuring device and a reference configuration where the transducers are uniformly distributed on the surface as shown in Fig. 1. Starting from time-of-flight inversion, we suggest reducing the optimization of the 3D configuration to a set of 2D OED problems using vertical and horizontal slices in a first step. This allows us to generate a good starting configuration for the 3D OED, which reduces the computational effort considerably. Based on this intermediate model we reiterate to determine the transducer locations in a fully 3D setup. Furthermore, we analyze to what extend the results from time-of-flight inversion can be carried over to waveform inversion.
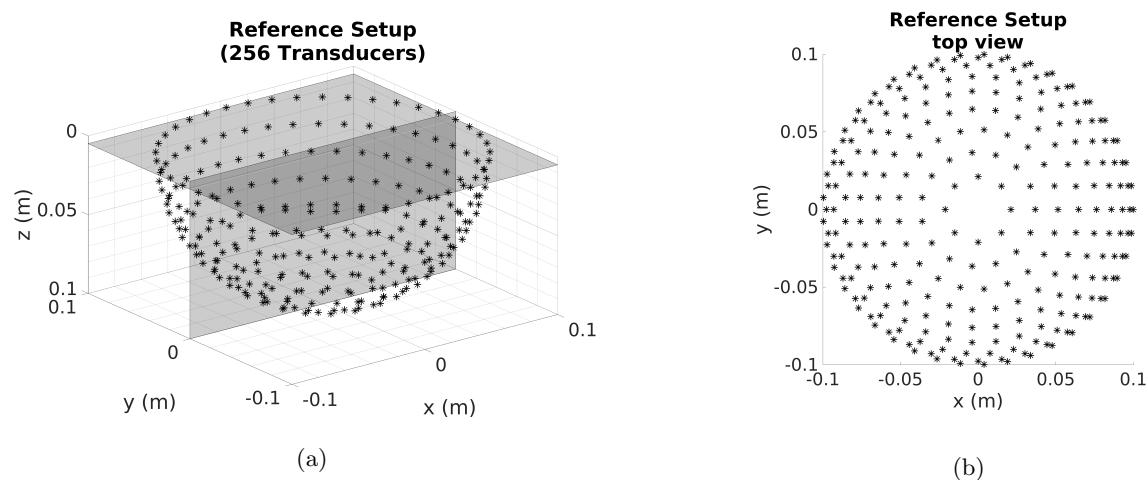


Figure 1: A hemispherically shaped measuring device covered by 256 uniformly distributed transducers. The planes indicate the horizontal and vertical slices considered for the OED problem in 2D.

This paper is organized as follows. First, we describe the theory and general formulation of Optimal Experimental Design and its application to straight ray time-of-flight inversion and waveform inversion, respectively. In a second step we propose a computationally tractable method to determine the transducer locations for 3D USCT. Finally, we show and discuss the configurations obtained using the suggested optimization strategy.

## 2. METHOD

### 2.1 Inverse problem

An essential component of imaging techniques is to use the physical relationship between measured ultrasound data $\mathbf{d_{obs}}$ and parameters $\mathbf{m}$ describing the acoustic properties of the tissue, e.g., sound speed. In general, this can be expressed in terms of a forward operator $\mathbf{F}$ that maps parameters $\mathbf{m}$ to data $\mathbf{d_{obs}}$,

$$\mathbf{d_{obs}} = \mathbf{F}(\mathbf{m}; \mathbf{S}). \tag{1}$$

Here, $\mathbf{F}$ depends on the experimental design $\mathbf{S}$, i.e., the position of emitting and receiving transducers. In the inverse problem, acoustic parameters are estimated by minimizing the least-squares misfit functional

$$\chi(\mathbf{m}; \mathbf{S}) = \frac{1}{2} \|\mathbf{d_{obs}} - \mathbf{F}(\mathbf{m}; \mathbf{S})\|^2 \tag{2}$$

constrained to our prior information on the tissue structure given by a regularization term $R(\mathbf{m})$. This yields the general formulation

$$\mathbf{m_{est}} = \arg\min \phi(\mathbf{m}), \qquad \phi(\mathbf{m}) = \chi(\mathbf{m}; \mathbf{S}) + \alpha R(\mathbf{m}). \tag{3}$$

The parameter $\alpha > 0$ balances the contribution of each term in the objective functional $\phi(\mathbf{m})$. The regularization term incorporates prior knowledge on the acoustic parameters (e.g., low-amplitude sound speed variations) to address the ill-posedness of the inverse problem and to avoid meaningless solutions. Common choices for $R$ are Tikhonov or total variation (TV) regularization[20] , which has been shown to be suitable for reconstructing the acoustic properties of breast tissue[21] and which we use in all numerical tests.

The Hessian matrix, i.e., the second derivatives of the objective function $\phi(\mathbf{m})$ with respect to the model parameters, can be split up into contributions from the misfit and the regularization term, respectively,

$$\phi''(\mathbf{m}; \mathbf{S}) = \chi''(\mathbf{m}; \mathbf{S}) + \alpha R''(\mathbf{m}). \tag{4}$$

In the context of Bayesian inference, where the estimated model parameters are interpreted in terms of probability density functions, the inverse of the Hessian matrix can be identified as the posterior covariance matrix. While this is exact only for a linear forward operator, the same strategy can be used for nonlinear operators as well to approximate the uncertainties in the vicinity of the minimum of the objective function $\phi(\mathbf{m})$.[22,23] The posterior covariance matrix provides a measure of how well the model parameters have been determined by the observed data and therefore, uncertainties in the estimated model parameters can be related to the spectrum of the Hessian,[24,25] which actually depends on the experimental design $\mathbf{S}$. Thus, by analyzing properties of the Hessian we can quantify the quality of a design.

Depending on the choice of the forward operator and the regularization term, solving the optimization problem (3) may require iterative methods and can be computationally very expensive. Therefore, ray-based methods are often used to linearize the forward operator with respect to the model parameters. To this end, we consider a time-of-flight inversion using straight rays. In this case $\mathbf{d_{obs}}$ corresponds to measured first-arrival times of flight, $\mathbf{m_{est}}$ describes the estimated slowness of the breast tissue, i.e., the inverse of sound speed, discretized in voxels of the numerical grid, and $\mathbf{F}$ is a matrix in which elements represent the length of the ray path traveling through each model parameter voxel. In this parameterization the forward operator is independent of the model parameters, i.e., $\mathbf{F} = \mathbf{F}(\mathbf{S})$ and the Hessian of the misfit term simplifies to $\chi''(\mathbf{m}; \mathbf{S}) = \mathbf{F}^T\mathbf{F}$.

Ray-based inversion methods are robust and computationally efficient but they suffer from a limited resolution caused by diffraction effects. Waveform tomography for USCT can overcome those limitations,[13–15,26] but

introduces a nonlinear operator $\mathbf{F} = \mathbf{F}(\mathbf{m}; \mathbf{S})$ governed by a partial differential equation. Here, we consider the acoustic wave equation for time-domain waveform inversion with a homogeneous density, which is given by

$$\frac{1}{(c(\vec{x}))^2}\frac{\partial^2}{\partial t^2}p(t, \vec{x}) - \Delta p(t, \vec{x}) = f(t, \vec{x}), \tag{5}$$

where $p(t, \vec{x})$ is the acoustic pressure field, $c(\vec{x})$ denotes the sound speed of breast tissue and $f(t, \vec{x})$ is the ultrasonic pressure source generated by transducers. In this case, the forward operator $\mathbf{F}$ in eq. (1) solves the time-domain acoustic wave equation and $\mathbf{d_{obs}}$ represents the acoustic pressure field measured by the receiving transducers. $\mathbf{m}$ contains the squared sound speed of breast tissue for all points of the numerically discretized grid. Due to the nonlinearity and the partial differential equation involved in the forward operator, there is no direct solution to the inverse problem available. Hence, iterative optimization methods are required to image the sound speed by solving the problem defined in eq. (3). However, properties of the Hessian can be estimated using matrix-free methods.[25] In particular, adjoint techniques allow us to compute Hessian-vector products at the cost of four wave propagation simulations per vector.[27, 28]

## 2.2 Optimal Experimental Design problem

The main idea of OED is to define a quality measure as a function of the design parameters that attains its maximal value when an experimental design maximizes the amount of information about the model that is expected to be contained in the measured data. The optimal design can then be found using a global optimization algorithm that searches among all possible designs subject to previously defined constraints – in our case possible transducer locations on the surface of the hemisphere. The two main challenges are (i) developing a suitable design criterion to characterize the information content and (ii) finding a computationally tractable method to determine the optimal design.

We propose to define the design quality measure based on the properties of the Hessian operator. As we pointed out in eq. (4), the Hessian of the objective function $\phi$ consists of two terms: $\chi''(\mathbf{m}; \mathbf{S})$, which includes the information on the model parameters for a given design $\mathbf{S}$, and $\alpha R''(\mathbf{m})$, which is related to the regularization term and represents our prior information on the acoustic properties of breast tissue. Because $R''$ does not depend on the design $\mathbf{S}$, we can focus on the misfit term. To simplify the notation we drop the dependency on $\mathbf{m}$ and $\mathbf{S}$ in the following and denote the Hessian of the misfit by $\mathbf{H}$. Note that in the time-of-flight inversion, we obtain $\mathbf{H} = \mathbf{F}^T\mathbf{F}$, where $\mathbf{F}$ only depends on $\mathbf{S}$, but not on the model parameters.

The quality of an experimental design can be improved by maximizing the contribution of $\mathbf{H}$ in $\phi''$. If $\mathbf{H}$ is decomposed numerically into its eigenvalues and eigenvectors, uncertainties in the model parameters will be related to the inverse of its eigenvalues.[17, 25] Therefore, if small eigenvalues exist, the inverse problem without regularization is ill-posed, the solution becomes unstable, and information about the model that is expected to be recovered from measurements is unreliable. Note that the regularization term essentially flattens the eigenvalue spectrum beyond a threshold value related to the regularization parameter $\alpha$, which is related to the noise level of the observed measurements. As a result, small eigenvalues are truncated to ensure a well-posed inverse problem, but there is no contribution to increase the model parameter resolution.

Typically, we can reduce the number of degrees of freedom in the inverse problem by truncating the domain to a smaller region of interest and use prior information, for instance, the sound speed of water in the exterior parts. The same reduction applies to the Hessian matrix as well. Several design quality measures were proposed by Curtis[18, 19] and Maurer et al.[17] trying to maximize the eigenvalues of $\mathbf{H}$ in a subspace that corresponds to our region of interest. Here, we use the following quality measure:

$$\Theta = \sum_{i=1}^{n}\frac{\lambda_i}{\lambda_1} = \frac{1}{\lambda_1}\text{trace}(\mathbf{H}_T), \tag{6}$$

where the eigenvalues $\lambda_i$ are sorted in order of decreasing magnitude, with $\lambda_1$ being the largest. The subscript $T$ indicates that the model space is truncated, with $n$ denoting the number of remaining parameters. Hence, we only consider elements in $\mathbf{H}$ that correspond to model parameters in the region of interest for computing the trace.

The quality measure in eq. (6) is normalized by the largest eigenvalue to avoid selecting configurations with only a few very large eigenvalues. This ensures that eq. (6) cannot be maximized by only increasing the information within a small part of the domain at the expense of a poor coverage of the rest. Fig. 2 illustrates a simple example for the linear case where the experimental design is determined by maximizing the quality measure in eq. (6) with and without normalizing by the largest eigenvalue. Other quality criteria are possible but require the computation of the complete eigenvalue spectrum, which is prohibitively expensive for large-scale problems.[18, 29]
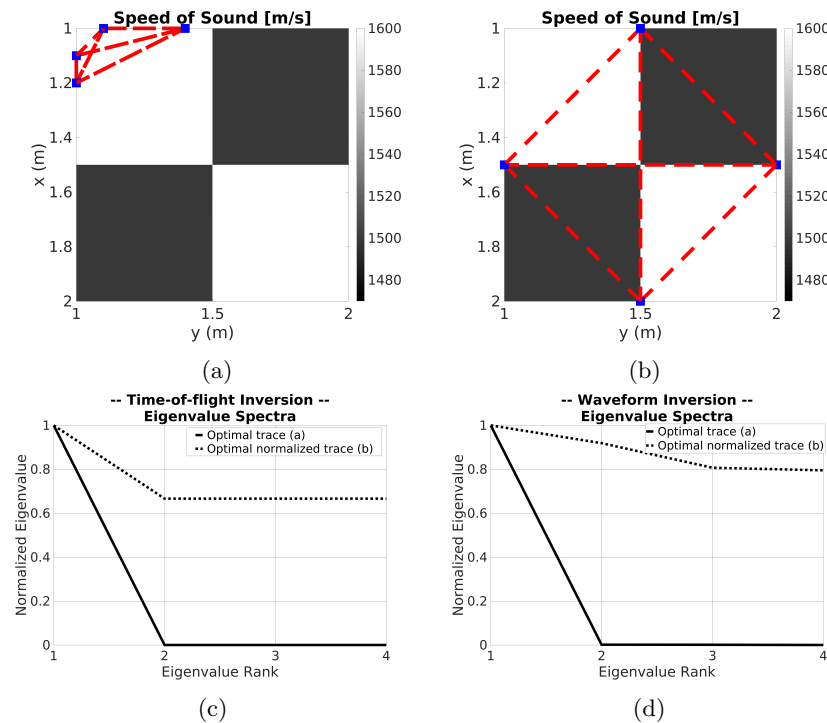


Figure 2: Optimal transducer locations considering time-of-flight inversion that (a) maximizes the trace of the Hessian or (b) maximizes the trace of the Hessian normalized by the largest eigenvalue. Transducers are represented by squares and straight ray paths by dashed lines. (c) Comparison between normalized eigenvalue spectra of $\mathbf{H}$, computed considering time-of-flight inversion, for both optimal solutions in (a) and (b). (d) Comparison between normalized eigenvalue spectra of $\mathbf{H}$, computed considering waveform inversion, for both optimal solutions in (a) and (b).

For nonlinear inverse problems the Hessian operator depends on both, the design and the model parameters. However, sound speed variations in the breast tissue are relatively small so that influential changes in the Hessian spectrum are not expected. This enables us to neglect the dependency on the model and to use the same quality measure for waveform inversion. Fig. 2d shows the corresponding normalized eigenvalue spectra of the Hessian operator for both experimental designs found in Fig. 2a and 2b. When comparing with Fig. 2c, similarities in both spectra suggest that time-of-flight inversion could provide a computationally tractable approximation to optimize the experimental design for waveform inversion approach. In addition, Table 1 shows the corresponding absolute and normalized values of the trace of the Hessian for both inversion approaches. In contrast to time-of-flight inversion, the configuration shown in Fig. 2b provides higher values in both quality criteria when waveform tomography is considered. Because the largest eigenvalue can only be approximated for waveform tomography, we consider the trace without normalization as design quality measure for waveform inversion in the following to avoid propagating numerical errors to the quality measure. This is known as A-optimal experimental design.[24, 25]

The trace of the Hessian matrix can be computationally intractable to compute in large-scale problems using waveform tomography. However, stochastic trace estimators have been successfully used for that purpose,[24, 25]

which only require a few Hessian-vector products, but not the full Hessian. In particular, we consider a variation of the trace estimation method proposed by Hutchinson,[30, 31] in which the trace of $\mathbf{H}$ is approximated by

$$\text{trace}(\mathbf{H}) \approx \frac{n}{N} \sum_{i=1}^{N} \frac{\mathbf{v_i}^T \mathbf{H} \mathbf{v_i}}{\mathbf{v_i}^T \mathbf{v_i}}, \tag{7}$$

where $\mathbf{v_i}$ are random vectors with values independently drawn from a normal distribution and $N$ is the sample size of the estimator, i.e., the number of random vectors.

| | Time-of-flight inversion | | Waveform inversion | |
|---|---|---|---|---|
| | trace | normalized trace | trace | normalized trace |
| Experimental Design Fig. 2a | 12 | 1 | 8.0643 | 1.0026 |
| Experimental Design Fig. 2b | 9 | 3 | 14.3615 | 3.5213 |

Table 1: Absolute and normalized values of the trace of the Hessian for experimental designs determined in Fig. 2 using time-of-flight and waveform inversion approaches.

## 2.3 Approachable experimental design

The quality measure in eq. (6) depends on the design parameters, i.e., transducer locations, in a highly non-linear manner. For that reason, in order to design an experiment, one should ideally exhaustively explore the entire space of all admissible combinations of design parameters. In geophysical applications a variety of global optimization algorithms have been used for this purpose.[29, 32–34] Here we consider Genetic Algorithms (GA)[35] to optimize eq. (6) with respect to the transducer locations (see Gallagher & Sambridge[36] for a detailed description of GA). In general, we may not find the globally optimal design but any increase in the quality measure will ensure an improvement in the reconstruction of the acoustic properties of the tissue. Furthermore, because it is a stochastic optimization method, GA may converge to different solutions in each run. Hence, we carry out the GA several times and use the result with the overall highest quality value.

The goal of our experiments is to determine the optimal locations of 256 transducers on the surface of a hemisphere (see Fig.1). An experimental design is described by a vector in which elements define the transducer locations in spherical coordinates. Due to the spherical symmetry of the scanning device, each position can be defined using only two coordinates: polar and azimuth angle. Therefore, we have a total of 512 design parameters. When the number of design parameters is as large as in this case, sampling the space of all possible experimental configurations by GA may be computationally infeasible. However, since the algorithm tends to preserve the information and structures contained in a successful design during the evolutionary process, the performance of GA could be sped up if an initial guess relatively close to globally optimal is available.

In order to get a good starting point for the global optimization, we suggest to exploit the azimuthal symmetry of our problem and solve only a set of 2D OED problems in vertical and horizontal planes. A 3D model of the transducer locations can then be obtained by combining the results from the individual slices. Note that GA samples the space of all possible experimental configurations and, thus, only forward problems are needed to evaluate the quality of each design. For large-scale nonlinear problems where the forward problem is expensive to compute, this approach helps us not only to reduce the design space but also to reduce the computational cost of successively solving the forward problem.

In the study presented here, the optimal experimental design problem is applied for time-of-flight tomography using straight-rays. Furthermore, we compare those configurations by computing the quality measure using waveform tomography. This helps us to analyze to what extend time-of-flight inversion gives a useful approximation to optimize the experimental design for waveform tomography. Note however, that extending the methodology presented above to waveform inversion is straightforward, but it requires significantly more computational resources.

# 3. RESULTS

The reference experimental design considered in this study is shown in Fig. 1. It consists of 256 transducers that are uniformly distributed on the surface of a hemisphere with a radius of 10 cm. To solve the forward problem described in eq. (1), and to evaluate the quality measure defined by eq. (6), the sound speed and the breast phantom is discretized with a rectilinear grid and a mesh-size of 2 mm. After optimizing the experimental design using the method described in the preceding section, the sound speed of breast tissue is reconstructed using the synthetic model shown in Fig. 3. Here we use a 3D numerical breast phantom based on the so-called Derenzo phantom[37] which is commonly used in medical imaging to test the spatial resolution of reconstructed images.
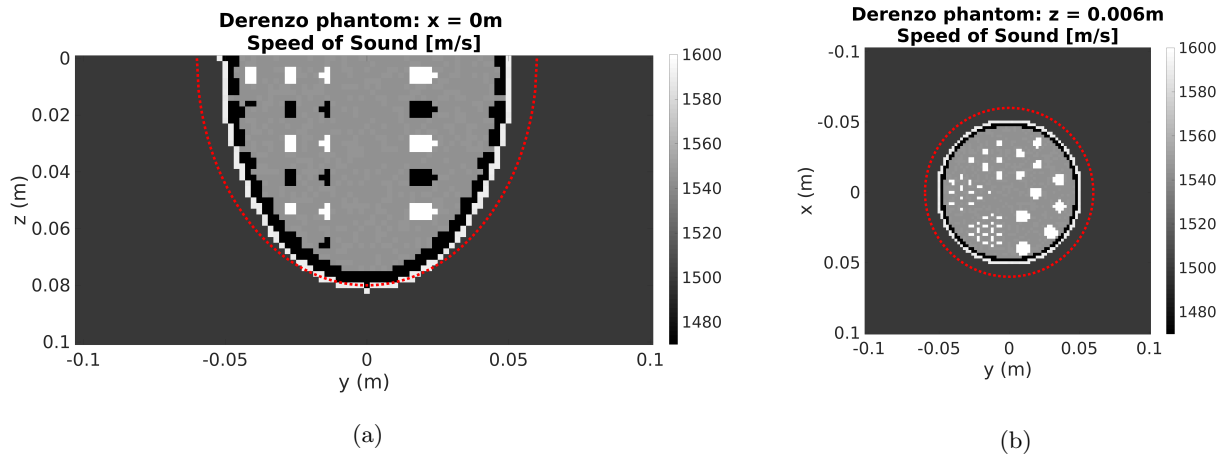


Figure 3: Derenzo phantom: (a) Vertical slice at $x = 0$ m and (b) horizontal slice at $z = 0.006$ m of the numerical breast model used for sound speed reconstruction. The dashed line next to the phantom indicates the region of interest in which we evaluate the quality measure.

As a first step to obtain a good starting configuration for the GA, we solve a set of OED problems for 2D time-of-flight inversion. First, we optimize the locations of transducers in the vertical direction. Here we consider 18 transducers, which corresponds to the total number of transducers defined in each slice of the reference experimental design in Fig. 1. Because the temperature of the surrounding water can be controlled and, thus, its exact acoustic properties are known, the quality measure is evaluated only in the subspace of the model where the breast is located. This defines the region of interest used in eq. (6). Once the optimized transducer locations are determined in the vertical direction, 12 horizontal slices corresponding to those elevations are considered. Fig. 4 shows the best configurations found by the GA for the vertical and horizontal slices indicated in Fig. 1.

A first general conclusion may be drawn from the solution in the vertical slice in Fig. 4b. The optimal configuration should gradually increase the spacing between the transducers from top to bottom. This compensates for the poor ray coverage in the upper part of the breast close to the chest wall, which is the case when the transducers are spaced uniformly, as shown in Fig. 4a. This design feature is intuitively understandable and can be generalized easily to a 3D configuration. Furthermore, Fig. 4e compares the corresponding normalized eigenvalue spectra for uniform and optimized designs. Higher values in the optimized case show that uncertainties in the parameters were decreased as expected. A larger number of significant eigenvalues indicates that the sound speed can indeed be better resolved.

In the horizontal plane, the optimized design suggests the need to break the symmetry of the uniform design in order to improve the ray coverage in the central part of the model. This can be seen in Fig. 4c-4d which shows the optimized configuration at an elevation of $z = 0.006$ m, i.e., the upper part of the breast close to the chest wall. The eigenvalue spectra of both designs, which are shown in Fig. 4f, look more similar in this case. However, there are two important improvements to note. First, the optimized configuration raises the level of the dominant eigenvalues in the normalized spectrum. Second, the number of significant eigenvalues is increased, which can be seen for rank 220 - 257. Similar features can be observed for other horizontal slices at different elevations.
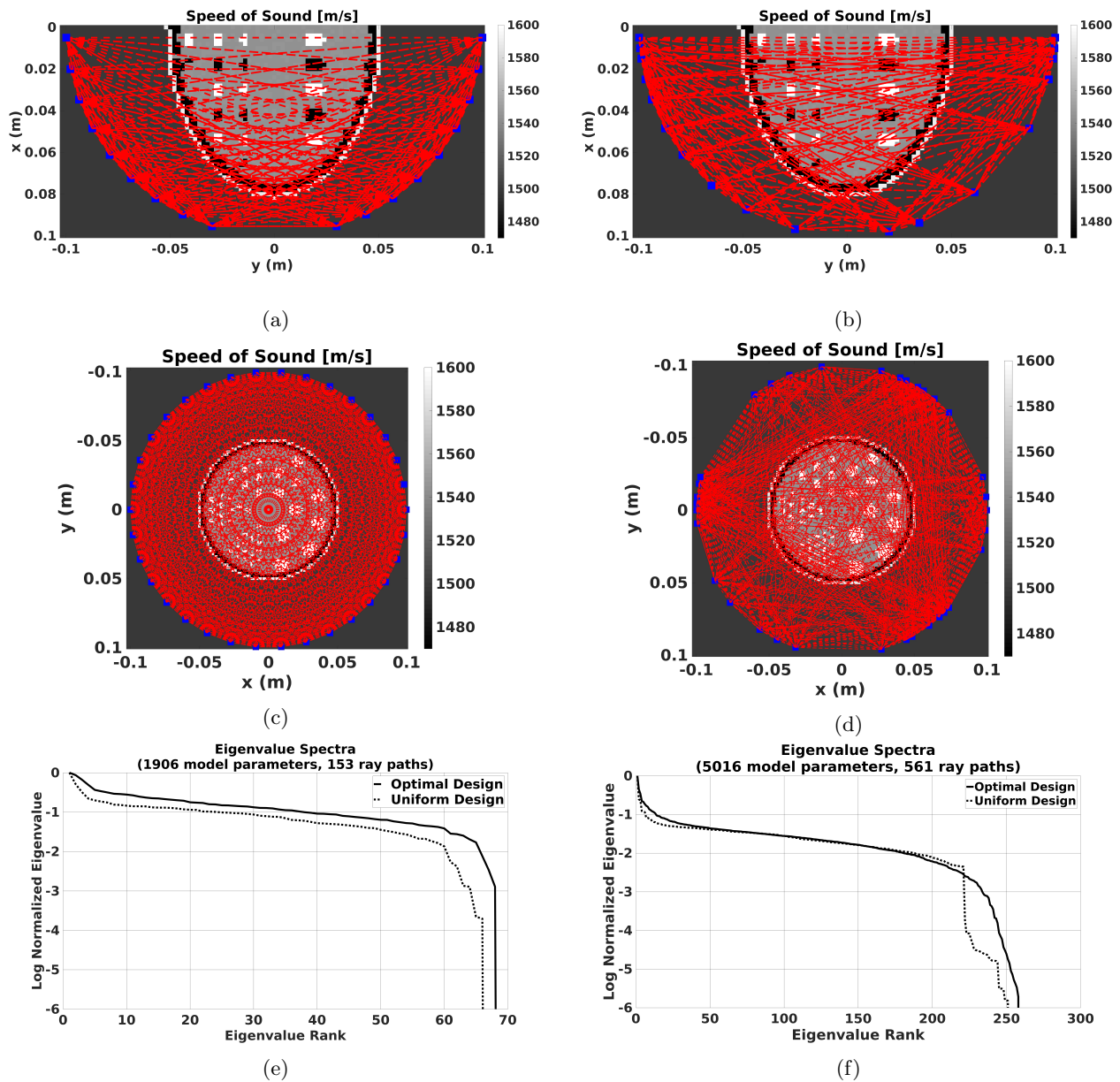
Figure 4: (a) Uniformly distributed reference configuration using 18 equidistantly spaced transducers (blue) and corresponding straight ray paths (red lines) for a 2D vertical slice at $x = 0$ m. A sound speed model of the breast has been included in the background for a better understanding of the experiment. (b) Optimized experimental design using eq. (6) for the vertical plane. (c) Uniformly distributed reference configuration using 34 transducers in a horizontal slice at $z = 0.006$ m. (d) Optimized transducer locations for the horizontal case. (e)-(f) Comparison of normalized eigenvalue spectra between uniform and optimized designs in the vertical and horizontal plane, respectively.

Based on these results, we construct a 3D configuration by stacking together the individual slices. The middle column in Fig. 5 shows the 3D design that is derived from the set of optimal solutions in the vertical and horizontal planes. The pattern we obtain significantly differs from the uniform configuration shown in the left column of Fig. 5. The new design is then used as initial guess for the global optimization in 3D, and

after executing it five times, the solution with the highest quality value is selected. Fig. 5c and Fig. 5f show the optimal 3D configuration resulting from the proposed OED problem in Sec. 2. Clearly, an interesting and initially non-intuitive pattern in the configuration is found by the algorithm: most of the transducers are gathered in three specific regions of the hemisphere, showing approximately a rotational symmetry of order three (angle of 120 degrees) with respect to the vertical axis. In addition, more transducers are located in the part of the hemisphere which is close to the chest wall, a feature that has been observed already in 2D OED problem for the vertical plane, see Fig. 4b.
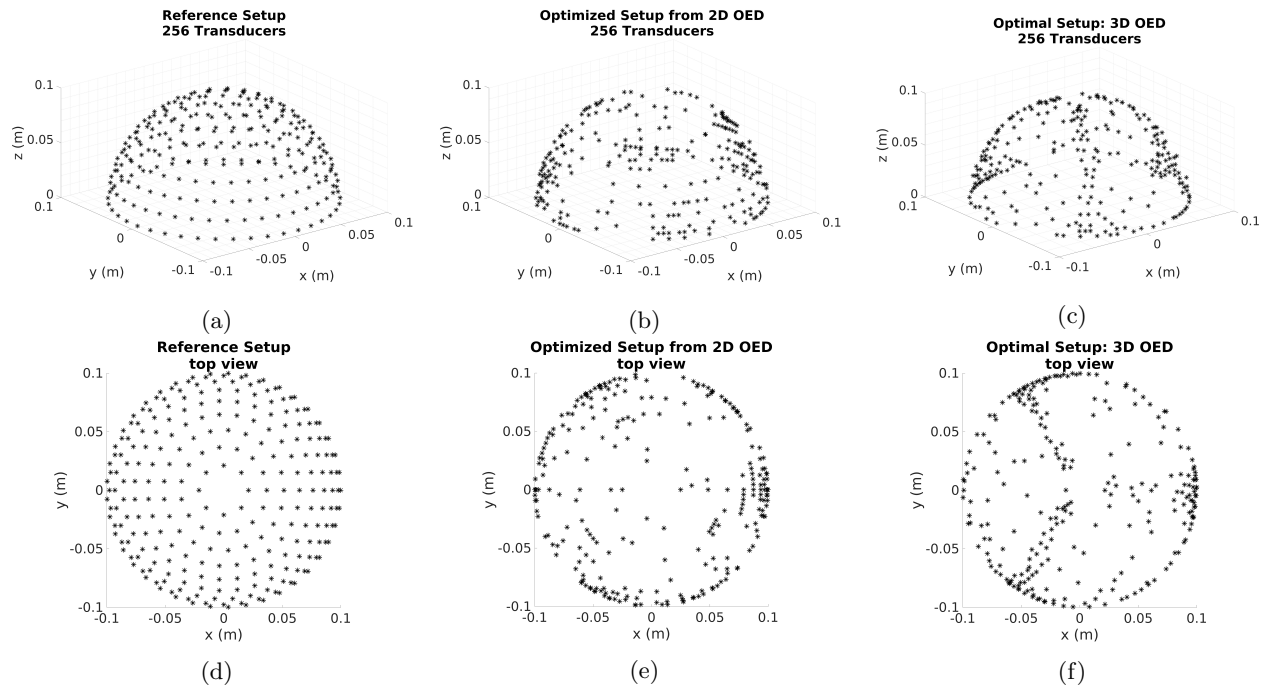


Figure 5: (a) Reference experimental design with uniformly distributed transducers. (b) 3D experimental design extrapolated from the 2D OED results. (c) Optimal 3D experimental design found by GA where the design in (b) was used as initial guess. (d)-(f) depict the top view of the configurations shown in (a)-(c).
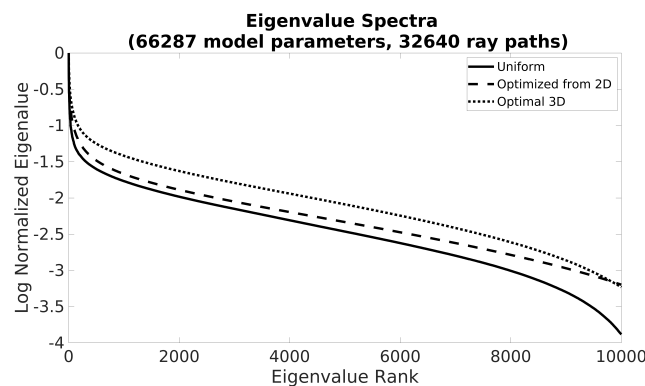


Figure 6: Comparison of normalized eigenvalue spectra between the uniform design (solid line), the optimized design constructed from the set of 2D OED problems using vertical and horizontal slices (dashed line) and the optimal design resulting from 3D global optimization (dotted line).

The comparison of the eigenvalue spectra shown in Fig. 6 indicates the benefits of OED and verifies our
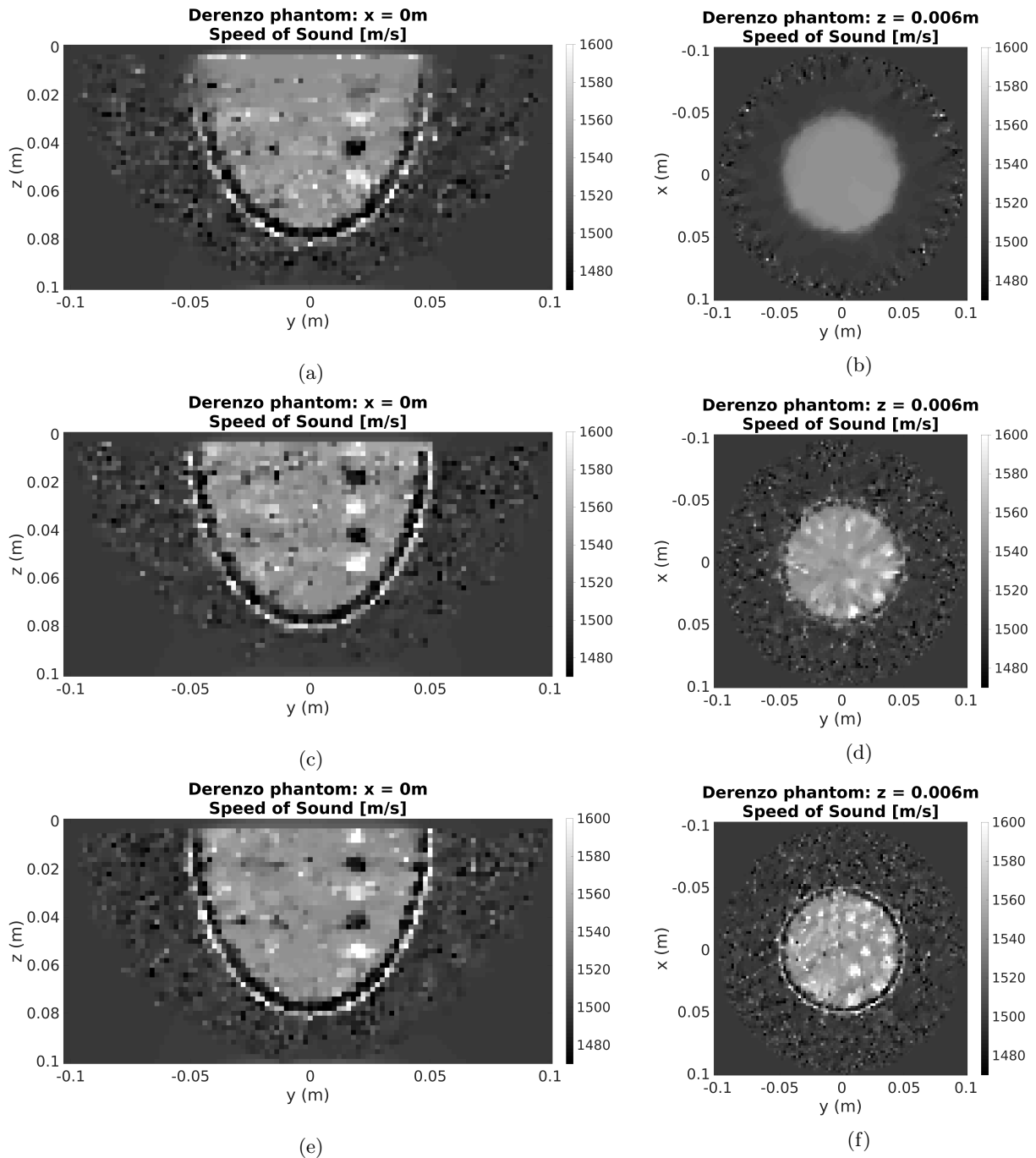
Figure 7: (g)-(i) Vertical slice at $x = 0$ m and (j)-(l) horizontal slice at $z = 0.006$ m showing the sound speed reconstructions obtained from the experimental designs in (a)-(c).

approach to start with sequentially optimizing 2D slices. The optimal experimental design does not only improve the relative values of the eigenvalues but also increases the number of significant eigenvalues, which allows us to collect information about the model that is missing in the reference configuration. However, we also observe trade-offs when comparing the eigenvalue spectra of the optimal experimental design with the design constructed from the intermediate 2D results. In particular, a higher design quality value does not necessarily imply a higher

number of significant eigenvalues. This corresponds to an increased resolution in some parts of the domain, at the expense of a poorer coverage in other parts.

To better understand the impact of the results, we compute sound speed reconstructions using the optimized experimental designs and compare them with the reference configuration. Time-of-flight measurements are collected using 3 rotations of the device, each one with an angle of 40 degrees and Gaussian noise with a standard deviation of 0.2% of the actual time-of-flights was added to the observations. Furthermore, the same regularization parameter is applied in the inverse problem defined in eq. (3) to give a fair comparison between the results of the different configurations. Note that rotations of the device were previously not included in the OED problem. However, rotations allow us to increase the number of measurements from new positions, but preserving the relative positions between the transducers.

Fig. 7 shows vertical and horizontal slices of reconstructions obtained from the reference uniform design, the 3D experimental design derived from sequential 2D optimizations, and the optimal design found by 3D global optimization, respectively. The images clearly show how the optimized configuration improves the region close to the chest wall, which is indeed of special interest in breast cancer detection. The uniform design fails in collecting information within the mentioned region. Hence, the sound speed reconstruction does not contain any fine-scale features and is merely the result of the regularization term.

## 4. DISCUSSION

The OED problem has been introduced and applied to determine the optimal transducer locations for ultrasound breast imaging. The efficiency of the method has already been demonstrated extensively in designing geophysical experiments. However, most geophysical exploration problems are tackled by two dimensional inversion approaches, which avoid the huge computational cost related to large-scale 3D problems. To this end, we proposed an approach that takes advantage of the radial symmetry of the scanning device.

The optimal design found using Genetic Algorithms, Fig. 5c and Fig. 5f, may not correspond to the global minimum of the design space. Nevertheless, the global optimization has been computed several times and it has been observed how all solutions share common features:

(i) many transducers are placed in the region close to the chest wall while their density is decreased gradually with elevation;

(ii) a rotational symmetry of order three with respect to the z-axis is found where most transducers are placed in only three specific regions of the hemisphere.

The same features are already observed in the 2D approximations of the experimental design that we performed in vertical and horizontal slices, see Fig. 4b and Fig. 4d respectively. The common features may therefore be used as rules of thumb in future experimental designs.

While the first feature is due to the poor ray coverage of the uniform design in the region close to the chest, which is in fact of special interest in breast cancer diagnosis, the second feature is less intuitive. In order to better understand it, we consider only one transducer in emitting mode as shown in Fig. 8a represented by a square. To facilitate the interpretation, a two-dimensional approximation of the problem is considered in the horizontal plane at $z = 0.006$ m corresponding to the upper part of the model. By definition, the quality measure in eq. 6 only considers ray paths intersecting with our region of interest (represented by a dashed circle), as the goal is to maximize information about the breast contained in the measured ultrasound data. Therefore, one could easily compute the tangent ray paths (solid lines) to our region of interest representing the limits within which any transducer in receiving mode would collect information about the breast. In other words, transducers placed outside of these limits would give us ray paths that do no intersect our region of interest and which therefore contain no information about the breast. The angle between the limits measured from the origin of reference system (dashed lines) is 120 degrees, which is consistent with the symmetry shown by the optimal experimental design found in Fig. 8b.

The applied design quality measure is sensitive only to the amount of information about the breast collected by measured ultrasound data. Further constraints or additional criteria, e.g., cost-related or task-based measures,

could be included in the methodology. This would either change the misfit functional and its Hessian or reduce the space of feasible design configurations. However, even without considering any further constraints, it is interesting to note that the resulting configuration follows a rather simple pattern. For instance, the scanning device could be approximately built using only four pieces: a ring shaped transducer holder in the region close to the chest wall and three plates of transducers following the features described in Fig. 8.
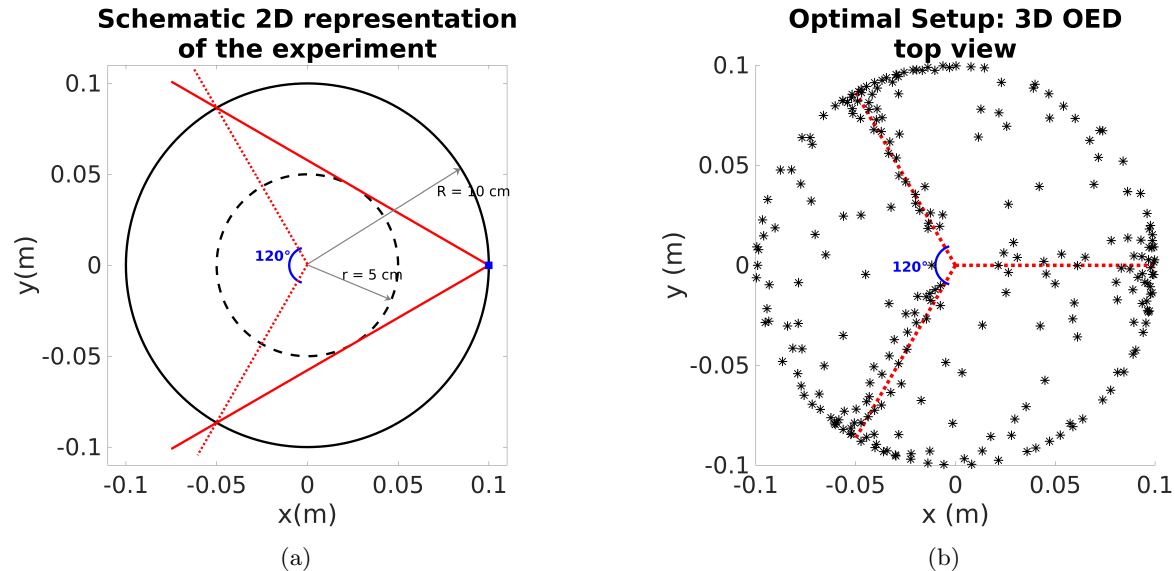


**Figure 8:** (a) Given an emitting transducer (square), the maximum angle between two receiving transducers for which ray paths (solid lines) intersect with our region of interest (dashed circle). The solid circle represents the device holding the transducers. (b) Top view of the optimal experimental design found in this study. Dashed lines with angular separation of 120 degree are overlaid to the final result.

The techniques presented herein were mainly considering time-of-flight inversions for reconstructing the sound speed of breast tissue. Therefore, only transmitted data was taken into account to determine the optimal design of the experiment. However, extensions of the OED problem to nonlinear problems, in particular to waveform tomography, were also introduced in Sec. 2.

It is difficult to assess to which extend the time-of-flight configuration can also yield an improved configuration for waveform inversion. Clearly, there are many more parameters involved, e.g., frequency of the transducers, selection of emitting transducers, emitted signal, misfit functional, simulation time, etc., that influence the result. Applying the A-optimal design criteria for the 2D vertical slice and the configurations shown in Fig. 4, we find that the optimal design for time-of-flight inversion indeed yields an improvement for waveform tomography compared to the uniform configuration. The estimated trace of the Hessian computed with adjoint methods using low-frequency transducers is 3.85 for the optimized and 3.46 for the uniform design, see Table 2. However, verifying the results in 3D is computationally challenging due to the tremendous cost of numerically simulating wave propagation in heterogeneous media and approximating the trace of the Hessian for many sources. Therefore, we consider three different experiments with either only one individual source or 40 sources with locations that are randomly selected from either the uniform or the time-of-flight optimal configuration. The results are summarized in Table 2. In general, both configurations give similar results in all tests, with each design giving slightly better values in two of the experiments. However, interpreting the results is difficult, because we only considered a small subset of sources and due to the aforementioned influence of other parameters. Analyzing the sensitivity of the quality criterion with respect to frequency and transducer size will be subject of further research.

In this study, we considered a fixed number of only 256 transducers to ensure a low cost experimental design since rotations allow us to have additional virtual locations for transducers. However, to estimate the minimum number of transducers needed to achieve the maximum benefit from an experiment, we are planning to apply

| Sources | Reference Setup | Optimal Setup |
|---|---|---|
| 2D, vertical slice | 3.46 | 3.85 |
| 3D, single source at $z = 0.075$ m | 4.86 | 4.83 |
| 3D, single source at $z = 0.097$ m | 4.90 | 5.00 |
| 3D, 40 sources | 15.17 | 15.03 |

Table 2: Estimates of the A-optimal design criterion evaluated for waveform tomography using either the reference setup or the optimal setups from time-of-flight inversion as shown in Fig. 4b and Fig. 5c, respectively.

sequential experimental design method in future studies. The method iteratively searches for the transducer location with the largest increase of the quality measure fixing the experimental setup of previous iteration.[38–40] If the number of transducers (the cost of an experiment), is represented graphically versus the respective value of the quality measure (quantitative benefit of an experiment), we expect to find Pareto-optimal points for which almost no significant increment in the quality value could be obtained when increasing the number of transducers. From there, a greater number of transducers is likely to result in increasingly redundant measurements.

## 5. CONCLUSIONS

We applied advanced methods of optimal experimental design to improve the transducer configuration for USCT. This provides a systematic and quantitative framework to increase the spatial resolution of the reconstruction without the need for additional measurements. Furthermore, these methods allow us to gain intuition about the design and to significantly reduce the computational cost of the inverse problems.

We observe that exploiting the radial symmetry enables us to start with a sequence of 2D problems that is then extended to a fully 3D design. The reconstructed images show the great potential of using non-uniform transducer locations in 3D ultrasound tomography scanning devices. We discovered an interesting pattern that clusters the transducers on a ring close to the chest wall and in three distinct areas on the hemisphere. The applicability of this design for waveform inversion is subject of future research. Further extensions of the method are possible to different design parameters (e.g., rotations, number of transducers) or tissue properties trying to constrain attenuation or density.

## ACKNOWLEDGMENTS

## REFERENCES

[1] André, M., Wiskin, J., and Borup, D., "Clinical results with ultrasound computed tomography of the breast," in [*Quantitative Ultrasound in Soft Tissues*], Mamou, J. and Oelze, M. L., eds., 395–432, Springer Netherlands, Dordrecht (2013).

[2] Ruiter, N. V., Zapf, M., Hopp, T., Dapp, R., Kretzek, E., Birk, M., Kohout, B., and Gemmeke, H., "3d ultrasound computer tomography of the breast: A new era?," *European Journal of Radiology* **81**, S133–S134 (2012).

[3] Jensen, J. A., Nikolov, S. I., Gammelmark, K. L., and Pedersen, M. H., "Synthetic aperture ultrasound imaging," *Ultrasonics* **44**, e5 – e15 (2006). Proceedings of Ultrasonics International (UI05) and World Congress on Ultrasonics (WCU).

[4] Duric, N., Littrup, P., Li, C., Roy, O., Schmidt, S., Seamans, J., Wallen, A., and Bey-Knight, L., "Whole breast tissue characterization with ultrasound tomography," in [*SPIE Medical Imaging*], 94190G–94190G, International Society for Optics and Photonics (2015).

[5] Huang, L., Shin, J., Chen, T., Lin, Y., Intrator, M., Hanson, K., Epstein, K., Sandoval, D., and Williamson, M., "Breast ultrasound tomography with two parallel transducer arrays: preliminary clinical results," *Proc. SPIE* **9419**, 941916–1–10 (2015).

[6] Greenleaf, J. F., Johnson, S. A., and Bahn, R. C., "Quantitative cross-sectional imaging of ultrasound parameters," in [*1977 Ultrasonics Symposium*], 989–995 (Oct 1977).

[7] Duric, N., Littrup, P., Babkin, A., Chambers, D., Azevedo, S., Kalinin, A., Pevzner, R., Tokarev, M., Holsapple, E., Rama, O., and Duncan, R., "Development of ultrasound tomography for breast imaging: Technical assessment," *Medical Physics* **32**(5), 1375–1386 (2005).

[8] Duric, N., Littrup, P., Poulo, L., Babkin, A., Pevzner, R., Holsapple, E., Rama, O., and Glide, C., "Detection of breast cancer with ultrasound tomography: First results with the Computed Ultrasound Risk Evaluation (CURE) prototype," *Medical Physics* **34**(2), 773–785 (2007).

[9] Zografos, G., Koulocheri, D., Liakou, P., Sofras, M., Hadjiagapis, S., Orme, M., and Marmarelis, V., "Novel technology of multimodal ultrasound tomography detects breast lesions," *European Radiology* **23**(3), 673–683 (2013).

[10] Duric, N., Littrup, P., Li, C., Roy, O., Schmidt, S., Cheng, X., Seamans, J., Wallen, A., and Bey-Knight, L., "Breast imaging with SoftVue: initial clinical evaluation," *Proc. SPIE* **9040**, 90400V–1–8 (2014).

[11] Ruiter, N. V., Gbel, G., Berger, L., Zapf, M., and Gemmeke, H., "Realization of an optimized 3D USCT," *Proc. SPIE* **7968**, 796805–1–8 (2011).

[12] Wiskin, J., Borup, D., Johnson, S., Andre, M., Greenleaf, J., Parisky, Y., and Klock, J., "Three-dimensional nonlinear inverse scattering: Quantitative transmission algorithms, refraction corrected reflection, scanner design and clinical results," *Proceedings of Meetings on Acoustics* **19**(1) (2013).

[13] Pratt, R. G., Huang, L., Duric, N., and Littrup, P., "Sound-speed and attenuation imaging of breast tissue using waveform tomography of transmission ultrasound data," *Proc. SPIE* **6510**, 65104S (2007).

[14] Wang, K., Matthews, T., ans C. Li, F. A., Duric, N., and Anastasio, M., "Waveform inversion with source encoding for breast sound speed reconstruction in ultrasound computed tomography," *IEEE Trans. Ultrason. Ferroelectr. Freq. Contr.* **62** (2014).

[15] Goncharsky, A., Romanov, S. Y., and Seryozhnikov, S. Y., "A computer simulation study of soft tissue characterization using low-frequancy ultrasonic tomography," *Ultrasonics* **67**, 136–150 (2016).

[16] Gemmeke, H., Dapp, R., Hopp, T., Zapf, M., and Ruiter, N. V., "An improved 3D ultrasound computer tomography system," *2014 IEEE International Ultrasonics Symposium* , 1009–1012 (2014).

[17] Maurer, H., Curtis, A., and Boerner, D. E., "Recent advances in optimized survey design," *Geophysics* **75**(5), 75A177–75A194 (2010).

[18] A.Curtis, "Theory of model-based geophysical survey and experimental design: Part 1 - Linear problems," *The Leading Edge* **23**(10), 997–1004 (2004).

[19] A.Curtis, "Theory of model-based geophysical survey and experimental design: Part 2 - Nonlinear problems," *The Leading Edge* **23**(10), 1112–1117 (2004).

[20] Jensen, T. L., Jørgensen, J. H., Hansen, P. C., and Jensen, S. H., "Implementation of an optimal first-order method for strongly convex total variation regularization," *BIT Numerical Mathematics* **52**(2), 329–356 (2012).

[21] Li, C., Duric, N., Littrup, P., and Huang, L., "In vivo breast sound-speed imaging with ultrasound tomography," *Ultrasound in Medicine and Biology* **35**(10), 1615 – 1628 (2009).

[22] Thacker, W. C., "The role of the Hessian matrix in fitting models to measurements," *Journal of Geophysical Research: Oceans* **94**(C5), 6177–6196 (1989).

[23] Fichtner, A. and Trampert, J., "Resolution analysis in full waveform inversion," *Geophysical Journal International* **187**(3), 1604–1624 (2011).

[24] Haber, E., Horesh, L., and Tenorio, L., "Numerical methods for experimental design of large-scale linear ill-posed inverse problems," *Inverse Problems* **24**(5), 055012 (2008).

[25] Alexanderian, A., Petra, N., Stadler, G., and Ghattas, O., "A fast and scalable method for A-optimal design of experiments for infinite-dimensional bayesian nonlinear inverse problems," *SIAM J. Sci. Comput.* **38**(1), A243–A272 (2016).

[26] Roy, O., Zuberi, M. A. H., Pratt, R. G., and Duric, N., "Ultrasound breast imaging using frequency domain reverse time migration," *Proc. SPIE* **9790**, 97900B–1–9 (2016).

[27] Fichtner, A. and Trampert, J., "Hessian kernels of seismic data functionals based upon adjoint techniques," *Geophysical Journal International* **185**(2), 775–798 (2011).

[28] Boehm, C. and Ulbrich, M., "A semismooth Newton-CG method for constrained parameter identification in seismic tomography," *SIAM Journal on Scientific Computing* **37**(5), S334–S364 (2015).

[29] Curtis, A., "Optimal experiment design: cross-borehole tomographic examples," *Geophysical Journal International* **136**(3), 637–650 (1999).

[30] Hutchinson, M., "A stochastic estimator of the trace of the influence matrix for laplacian smoothing splines," *Communications in Statistics - Simulation and Computation* **19**(2), 433–450 (1990).

[31] Avron, H. and Toledo, S., "Randomized algorithms for estimating the trace of an implicit symmetric positive semi-definite matrix," *J. ACM* **58**(2), 8:1–8:34 (2011).

[32] Hardt, M. and Scherbaum, F., "The design of optimum networks for aftershock recordings," *Geophysical Journal International* **117**(3), 716–726 (1994).

[33] Ajo-Franklin, J. B., "Optimal experiment design for time-lapse traveltime tomography," *Geophysics* **74**(4), Q27–Q40 (2009).

[34] Roux, E. and Garcia, X., "Optimizing an experimental design for a CSEM experiment: methodology and synthetic tests," *Geophysical Journal International* **197**, 135–148 (2014).

[35] Chipperfield, A. J. and Fleming, P. J., "The MATLAB genetic algorithm toolbox," in [*IEE Colloquium on Applied Control Techniques Using MATLAB*], 10/1–10/4 (Jan 1995).

[36] Gallagher, K. and Sambridge, M., "Genetic algorithms: A powerful tool for large-scale nonlinear optimization problems," *Computers and Geosciences* **20**(7), 1229 – 1236 (1994).

[37] Derenzo, S. E., Budinger, T. F., Huesman, R. H., Cahoon, J. L., and Vuletich, T., "Imaging properties of a positron tomograph with 280 BGO Crystals," *IEEE Transactions on Nuclear Science* **28**, 81–89 (Feb 1981).

[38] Curtis, A., Michelini, A., Leslie, D., and Lomax, A., "A deterministic algorithm for experimental design applied to tomographic and microseismic monitoring surveys," *Geophysical Journal International* **157**(2), 595–606 (2004).

[39] Guest, T. and Curtis, A., "Iteratively constructive sequential design of experiments and surveys with nonlinear parameter-data relationships," *Journal of Geophysical Research: Solid Earth* **114**(B4), n/a–n/a (2009). B04307.

[40] Maurer, H., Greenhalgh, S., and Latzel, S., "Frequency and spatial sampling strategies for crosshole seismic waveform spectral inversion experiments," *Geophysics* **74**(6), WCC79–WCC89 (2009).